ELECTRICAL PROPERTIES OF THE MYOTENDON REGION OF FROG TWITCH MUSCLE FIBERS MEASURED IN THE FREQUENCY DOMAIN

RICHARD L. MILTON, RICHARD T. MATHIAS, AND ROBERT S. EISENBERG
Department of Physiology, Rush Medical College, Chicago, Illinois 60612

ABSTRACT The electrical properties of the end of a muscle fiber were determined using three microelectrodes, one passing sinusoidal current, the other two recording the resulting voltages. An electrical model was constructed from the morphology of the fiber, including the resistance of the extracellular space between cells; the parameters of this model were determined by fitting the model to the observed voltage responses. Our results, analyzed directly or by curve fits, show that the end of muscle fibers contains a large capacitance resulting from the extensive membrane folds at the myotendon junction. Analysis and simulations show that the extra capacitance at the myotendon junction has substantial effects on measurements of linear properties, in particular on estimates of the capacitance of the membranes. There is little qualitative effect on classical measurements of nonlinear charge movement (provided they were made with one set of electrode locations) if the linear components have been subtracted. Quantitative estimates of nonlinear charge movement and ionic currents are significantly affected, however, because these estimates are customarily normalized with respect to the linear capacitance.

INTRODUCTION

The voltage-dependent properties of skeletal muscle fibers have been extensively studied with a voltage clamp method that exploits the special properties of the end of an idealized one-dimensional electrical cable, a cable assumed to have no longitudinal current flow at its termination (Adrian and Freygang, 1962; Adrian et al., 1970; Schneider and Chandler, 1973; Horowicz and Schneider, 1981; many other papers reviewed in Almers, 1978; Schneider, 1981, and Adrian, 1984). The longitudinal variation in intracellular potential in such an idealized fiber is small near its termination and the first-order variation in potential that does occur provides a good estimate of the current flow across the fiber membranes.

A muscle fiber is not necessarilly an idealized cable, however, and so we thought it worthwhile to use the high resolution technique of frequency domain analysis (reviewed in Eisenberg, 1984*a*, *b*; Mathias, 1984) to measure the current flow at the end of the fiber. Our measurements reveal a surprisingly large current, a capacitive current that presumably flows across the extra membrane found at the myotendon junction (Eisenberg and Milton, 1984). This capacitive current flow has a profound effect on estimates of the linear electrical properties of muscle fibers (Schneider and Chandler, 1976; Chandler and Schneider, 1976) and on measurements taken at more than one set of electrode locations. It has no significant effect on qualitative estimates of nonlinear charge movement; quantitative estimates of charge movement are affected because the normalization by linear capacitance is affected.

GLOSSARY

a	radius of fiber (centimeters)
C_{en}	capacitance of membranes at myotendon junction in a unit fiber cross-sectional area (farad per centimeter squared)
G_{en}	conductance of membranes at myotendon junction in a unit fiber cross-sectional area (siemens per centimeter squared)
$Im(\,)$	the imaginary part of complex quantity within the parentheses
I_0	total current injected into fiber (amperes)
j	$\sqrt{-1}$
L	distance from current passing electrode to the end of the fiber, $L > 0$ (centimeter)
L'_1, L'_2	locations on the central (i.e., proximal) side of the current electrode, the side away from the fiber end; L'_1, L'_2 are positive numbers (centimeters)
L_1, L_2	locations distal to the current electrode, between the current electrode and the end of the fiber; L_1, L_2 are both positive numbers $<L$ (centimeters)
$Re(\,)$	the real part of the complex quantity within the parentheses
r_i	longitudinal resistance of 1 cm of fiber sarcoplasm, called the sarcoplasmic resistance $r_i = Re(z_i)$ (ohms per centimeter)
R_{ae}	access resistance in series with membranes at myotendon junction for a unit cross-sectional area of fiber (ohms times centimeter squared)
V_1, V_2	intracellular potentials at locations L_1, L_2 shown in Fig. 1 (volts) (Note the subscripts identify the location at which the potential is recorded, not the electrode that records the potential.)
V_{FF}	potential at a location indicated in Fig. 2: output of the feedback follower, an approximation to the membrane potential, see Eq. 1
V'_1, V'_2	intracellular potentials at locations L'_1, L'_2 shown in Fig. 1 (volts). (Note the subscripts identify the location at which

the potential is recorded, not the electrode that records the potential.)

V_{en} intracellular potential at the end of the fiber, $V_{en} = V_m(-L, j\omega)$, see Fig. 1 (volts)

$V_m(x, j\omega)$ intracellular potential at location x (volts)

V_{NC} potential at location indicated in Fig. 2: output of negative capacity amplifier, an approximation to the longitudinal gradient of potential ΔV, see Eq. 2

x longitudinal distance along fiber length from reference point, the point of current injection (centimeters)

y_{en} admittance of all membranes at myotendon junction, see Eq. 3. (siemens)

y_m shunt admittance (to radial current) in 1 cm of fiber length. (siemens per centimeter)

z_i longitudinal impedance of 1 cm of sarcoplasm, called the sarcoplasmic impedance (ohms per centimeter)

ΔV or $\Delta V'$ longitudinal gradient of potential between two locations $\Delta V = V_2 - V_1$; $\Delta V' = V_2' - V_1'$ (volts)

Γ propagation constant $= (z_i y_m)^{1/2}$, a frequency dependent quantity (centimeter^{-1})

τ_{FF} time constant formed by the resistance and stray capacitance associated with the microelectrode connected to amplifier A in Fig. 2 (see Milton, 1984, for details) (seconds)

τ_{NC} time constant formed by the resistance and uncompensated capacitance (namely, the stray capacitance) associated with the electrode connected to amplifier F in Fig. 2 (see Milton, 1984, for details) (seconds)

ω angular frequency (radians per seconds).

METHODS

Measurements were made on sartorius muscle fibers of frogs of the species *Rana temporaria* bathed in $[Na^+] = 120$ mM, $[K^+] = 2.5$, $[Ca^{++}] = 1.8$, $[Cl^-] = 121$, $[H_2PO_4^-] = 0.85$, $[HPO_4^-] = 2.15$, $[TTX] = 1.5 \times 10^{-6}$ M, pH = 7.2 (set by the addition of small amounts of HPO^-_4). The muscle was stretched to some 1.3 times rest length. At the completion of each experiment the whole sartorius muscle was fixed for ~30 min in a solution of 5% (wt/vol) glutaraldehyde in a buffer (pH = 7.2) of 100 mM Na^+ cacodylate and 1.8 $CaCl_2$ and stored at 4°C in a buffer (pH = 7.2) of 100 mM Na^+ cacodylate, 292 sucrose, and 1.8 $CaCl_2$. Individual fibers were then teased out of the whole muscle (usually three per muscle) and their sarcomere spacings measured using phase contrast optics. Microelectrodes, prepared and shielded as described in Mathias et al. (1977) were placed in the locations shown in Fig. 1. Some difficulty was found in determining the location of the end of the fiber, particularly because of the large variation in taper from fiber to fiber. The procedure followed in these experiments was to locate the most distal end of the fiber and then assume the electrical end of the fiber (i.e., $x = -L$ in Fig. 1 and subsequent equations) to be one fiber radius from this most distal point.

We used novel circuitry designed to maintain one point in the fiber at nearly ground potential. The potential at a neighboring point is then a direct measure of the potential drop in the fiber interior. This arrangement serves to increase bandwidth and common mode rejection, while decreasing circuit cost and complexity.

Feedback Follower

The feedback follower (Eisenberg and Gage, 1969; Mathias et al., 1979) was one of two circuits used to measure intracellular potential. In this circuit the microelectrode, fiber membrane, and bath electrode are placed in the feedback loop of an operational amplifier, as shown on the left-hand side of Fig. 2. This arrangement maintains the top of the microelectrode at virtual ground thus minimizing the driving force for current through the capacitance to ground. The gain of this circuit is approximately

$$-V_{FF} = \frac{V_m(x, j\omega)}{1 + j\omega\tau_{FF}} \tag{1}$$

(assuming that potential drops in the bathing solution and across the bath electrode are negligible). Capacitive coupling between the electrode interior and the bathing solution causes the deviation (described in Eq. 1) from the actual intracellular potential, the effect being particularly evident at higher frequencies. This deviation was removed analytically from the data by applying a calibration voltage to the inverting input of the feedback follower amplifier (terminal V_{c_1} in Fig. 2) and determining τ_{FF}. Details of this procedure are given in Milton (1983).

Negative Capacitance Follower

A second amplifier was needed to record the voltage on the second microelectrode: the feedback follower circuit could not be used because only one point in the fiber may be held at virtual ground. The standard voltage follower configuration of operational amplifiers does not give adequate bandwidth for our purposes because of the amplifier's input capacitance and so, following a well-trodden path, we constructed a negative capacitance follower. We added a feedback path, between the output and noninverting input of a voltage follower, containing a noninverting amplifier (gain 2) in series with a variable capacitor (Fig. 2). This capacitor can be adjusted to compensate for current through the follower's input capacitance, thus greatly extending the bandwidth of the circuit. Bandwidths of ~50 kHz are easily obtained.

Only the amplifier's input capacitance to ground was compensated; no attempt was made to compensate for the capacitance between the electrode interior and the bath (it is theoretically not possible to do so unless the potential drops in the bath are known: Valdiosera et al., 1974*a*); the uncompensated capacitance was reduced by a driven shield and residual effects on the data were removed by applying a calibration voltage (to terminal V_{c_2} in Fig. 2) and determining τ_{NC} (details in Milton, 1983).

When current is injected into the fiber, the voltage perturbation measured with the negative capacitance follower is

$$V_{NC} = \frac{V_2}{1 + j\omega\tau_{NC}} - \frac{V_1}{1 + j\omega\tau_{FF}}. \tag{2}$$

(This equation assumes that the fiber has also been impaled with the feedback follower electrode and that any current passing through the amplifier's input capacitance to ground has been compensated). Data collection and analysis followed the procedures described in detail in Mathias et al. (1977) and Milton (1983).

Fig. 3 shows the circuit used to represent the end of the fiber. Note that the parameters R_{se} (series resistance: ohms times centimeter squared), G_{en}

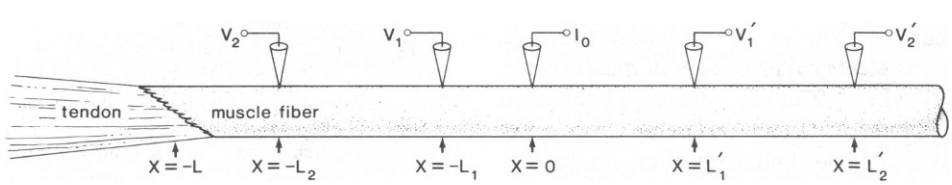

FIGURE 1 Electrode placements used in fiber center and at fiber end. L varied between 468 and 1,194 μm. L_1 varied between 115 and 439 μm. L_2 varied between 573 and 919 μm. L_1' varied between 115 and 296 μm. L_2' varied between 200 and 458 μm.

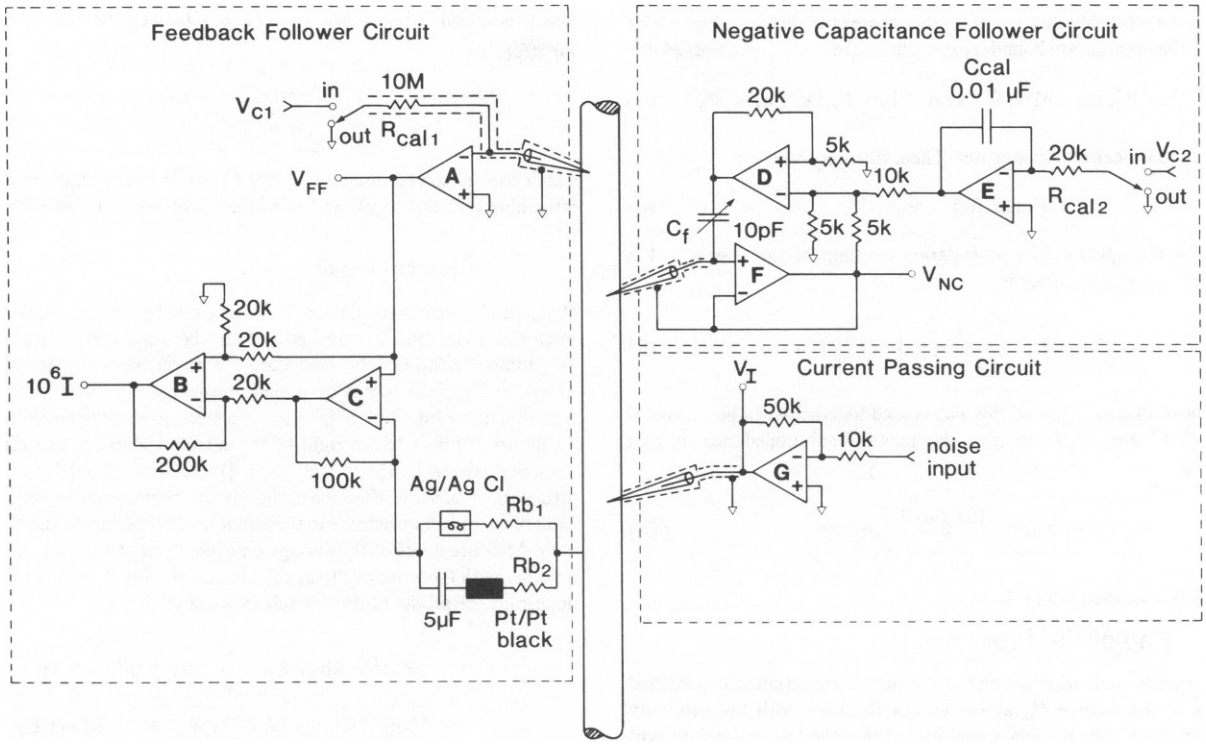

FIGURE 2 Circuitry used to inject current and measure voltage response. Amplifiers A-F were operational amplifiers (model no. 48K; Analog Devices, Inc., Norwood, MA), Amplifier G was a ± 100 V operational amplifier (model no. 1022, Teledyne Philbrick Co., Dedham, MA), dotted lines surrounding electrodes represent conductive shielding.

(membrane conductance: siemens per centimeter squared) and C_{en} (membrane capacitance: farads per centimeter squared) are referred to the cross-sectional area of the fiber but that the admittance of the end of the fiber y_{en} is given in absolute units siemens. Thus,

$$y_{en} = \frac{\pi a^2}{R_{se} + \dfrac{1}{G_{en} + j\omega C_{en}}}. \tag{3}$$

The values of C_{en}, G_{en}, and R_{se} were estimated from the following approximate relationships

$$C_{en} \approx \frac{Im(y_{en})}{(\pi a^2)\omega}; \quad \text{for } 50 \le \frac{\omega}{2\pi} \le 100 \text{ Hz.}$$

$$G_{en} \approx \frac{Re(y_{en})}{\pi a^2}; \quad \text{for } 5 \le \frac{\omega}{2\pi} \le 25 \text{ Hz.} \tag{4}$$

$$\frac{R_{se}}{\pi a^2} \approx \frac{1}{\omega C_{en}} [-1 + (\pi a^2)\omega C_{en}/Im(y_{en})]^{1/2},$$

$$\text{for } 500 \le \frac{\omega}{2\pi} \le 1{,}000 \text{ Hz.}$$

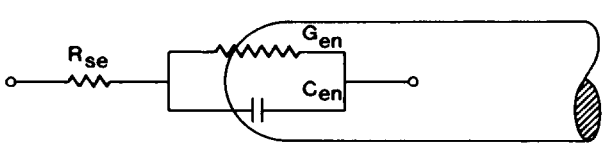

FIGURE 3 Circuit model representing the admittance y_{en} of the end of the fiber.

The right-hand side of Eq. 4 represents the frequency ranges over which the experimental data were averaged to obtain a direct estimate of the parameters on the left-hand side of the equation.

THEORY

An essential step in the measurement of electrical properties is the construction of a structural model, which is used to relate the measured voltage and current to the electrical properties of muscle fiber components. We represent the properties of a muscle fiber by a one-dimensional cable equation (Jack et al., 1975), which has been shown to be an adequate representation of a muscle fiber by Schneider (1970), Hodgkin and Nakajima (1972), and Valdiosera et al., (1974*b*,*c*).

$$\frac{1}{\Gamma^2}\frac{d^2 V_m(x, j\omega)}{dx^2} - V_m(x, j\omega) = 0. \tag{5}$$

The general solution can be written as

$$V_m(x, j\omega) = A^{\pm}(j\omega) \sinh [x\Gamma(j\omega)] + B^{\pm}(j\omega) \cosh [x\Gamma(j\omega)], \tag{6}$$

where $A^{\pm}(j\omega)$ and $B^{\pm}(j\omega)$ are unknown constants (the positive superscript for positive x, negative for negative x) to be determined by the boundary conditions that describe the microelectrode source of current and the end of the fiber.

We now perform an inverse analysis using the general solution and boundary conditions to determine the sarcoplasmic impedance of the fiber $z_i(j\omega)$ and the propagation constant $\Gamma(j\omega)$, given measurements of the applied current I_0 and voltages indicated in Fig. 1. The properties of the components of the fiber will in turn be determined from z_i and Γ, using a model of the electrical structure of the fiber fit to our experimental data.

When the electrodes are near the fiber center (as shown in Fig. 1 with $L \to \infty$), the appropriate boundary conditions are

$$\lim_{x \to \pm\infty} V_m(x, j\omega) = 0 \quad \text{and} \quad \lim_{|x| \to 0} V_m(x, j\omega) = V_0, \qquad (7)$$

where $x = 0$ is near the fiber center. Then, Eq. 6 becomes

$$V_m(x, j\omega) = V_0 e^{-\Gamma|x|}, \qquad (8)$$

with $V_0 = (I_0 z_i)/(2\Gamma)$. The propagation constant of the fiber $\Gamma(j\omega)$ is estimated at each frequency by

$$\Gamma(j\omega) = \frac{1}{(L_2' - L_1')} \ln (V_2'/V_1'). \qquad (9)$$

The value of $\Gamma(j\omega)$ computed this way is used together with the measured values of L_1' and V_1'/I_0 to give the longitudinal impedance at that frequency

$$z_i(j\omega) = \frac{2\Gamma(j\omega)\, V_1'}{I_0} e^{L_1'\Gamma(j\omega)}. \qquad (10)$$

L_2' and L_1' are defined in Fig. 1.

End of the Fiber

Measurements made near the end of the fiber are conveniently analyzed in terms of the voltage V_{en} at the end of the fiber with the geometry defined in Fig. 1. The boundary condition is that the longitudinal current equals the current through the admittance of the membranes at the end of the fiber

$$\lim_{x \to -L} \frac{1}{z_i} \frac{dV_m(x, j\omega)}{dx} = V_{en} y_{en}, \text{where } V_{en} \equiv \lim_{x \to -L} V_m(x, j\omega). \qquad (11)$$

The solution to the cable equation then becomes

$$V_m(x, j\omega) = V_{en}\left\{\cosh \Gamma(x + L) + \left[\frac{y_{en} z_i}{\Gamma}\right] \sinh \Gamma(x + L)\right\} \quad \text{for } -L \le x \le 0. \qquad (12)$$

Although the expressions in Eqs. 8–10 were derived for the case where the electrodes are near the center of the fiber, they are valid near the end of the fiber in the region to the right of the current electrode $x > 0$, if the preexponential factor V_0 is redefined as

$$V_m(x, j\omega) = V_0^* e^{-\Gamma x}; \quad \text{for } x \ge 0$$

$$\text{where } V_0^* = V_{en}\left[\cosh (\Gamma L) + \frac{y_{en} z_i}{\Gamma} \sinh (\Gamma L)\right]. \qquad (13)$$

We can relate the total current injected into the fiber I_0 to the potential (e.g., at the end of the fiber) by (*a*) determining the longitudinal current leaving the electrode (in both directions) using Ohm's law to compute the derivatives $(dV/dx)_{\pm 0}$ on either side of the current electrode or by (*b*) determining the sum of the current across the end of the fiber and the integral of the current density crossing the membrane (namely, the integral of $y_m V_m$ from $x = -L$ to 0 and then from $x = 0$ to ∞). Either way

$$I_0 = V_{en}\left(\frac{\Gamma}{z_i} + y_{en}\right) e^{\Gamma L}. \qquad (14)$$

Classical Case

We now determine fiber properties from our data with the classical assumption of no current flow at the end of the fiber. For recording locations shown in Fig. 1 as $x = -L_1$ and $-L_2$, we have from Eq. 12 with $y_{en} = 0$

$$\frac{V_1}{V_2} = \frac{\cosh \Gamma(L - L_1)}{\cosh \Gamma(L - L_2)}, \qquad (15)$$

which can be solved numerically for $\Gamma(j\omega)$ at each frequency $j\omega$. The remaining variable $z_i(j\omega)$ can be determined by Eq. 17 below with $y_{en} = 0$.

General Case

If y_{en} is to be measured and not just assumed to be zero, at least one of the microelectrodes must be removed and the fiber repenetrated at a different longitudinal location. The procedure for direct measurement of $\Gamma(j\omega)$, $z_i(j\omega)$, and $y_{en}(j\omega)$ begins by making measurements of V_1' and V_2' (and thus $\Gamma(j\omega)$: see Eq. 9) with the recording electrodes at the positions L_1' and L_2' shown in Fig. 1 to the right of the current electrode. The remaining variables (namely, $z_i[j\omega]$ and $y_{en}[j\omega]$) are determined by additional measurements, made after one of the voltage electrodes is moved from the right of the current electrode to the left of the current electrode, from L_1' to $-L_1$. Measurements of the voltage on each electrode at each frequency, together with the value of $\Gamma(j\omega)$ calculated from Eq. 9 at each frequency, determine the product (also at each frequency)

$$z_i y_{en} = \Gamma \frac{e^{-\Gamma L_2'} \cosh (\Gamma L) - \dfrac{V_2'}{V_1} \cosh [\Gamma(L - L_1)]}{\{V_2'/V_1\} \sinh [\Gamma(L - L_1)] - e^{-\Gamma L_2'} \sinh (\Gamma L)}. \qquad (16)$$

z_i itself can be determined from this product

$$z_i(j\omega) = \frac{\{V_1/I_0\} \Gamma e^{\Gamma L}\left[1 + \left(\dfrac{z_i y_{en}}{\Gamma}\right)\right]}{\cosh [\Gamma(L - L_1)] + \left(\dfrac{z_i y_{en}}{\Gamma}\right) \sinh [\Gamma(L - L_1)]}. \qquad (17)$$

All the information required to evaluate the right-hand side of this equation (at each frequency) is known. The product $z_i y_{en}$ is known from Eq. 16, $\Gamma(j\omega)$ is known from Eq. 9, and V_1/I_0 is measured.

RESULTS

We seek to determine the electrical properties of the membranes at the myotendon junction from measurements of the fiber's voltage response to applied sinusoidal current. The voltage responses measured from electrode penetrations in the fiber center are compared with those measured at the fiber end. Differences between these responses from fiber center and end are interpreted as the result of current flow at the myotendon junction.

Electrodes Near the Middle of the Fiber

Measurements of $V_1'/\Delta V'$ and V_1'/I_0 were made over a frequency range of 0 to 2,000 Hz with three microelectrodes impaled in the middle of the fiber as described in the Theory section (see Fig. 1, with $L \to \infty$). A circuit model of the fiber was fit to these measurements (Fig. 4) and the resulting best fit estimates of the parameters of the circuit (Table I) were compared with values obtained at the fiber end.

The measurements were also used to generate plots of the longitudinal impedance of the sarcoplasm of the fiber,

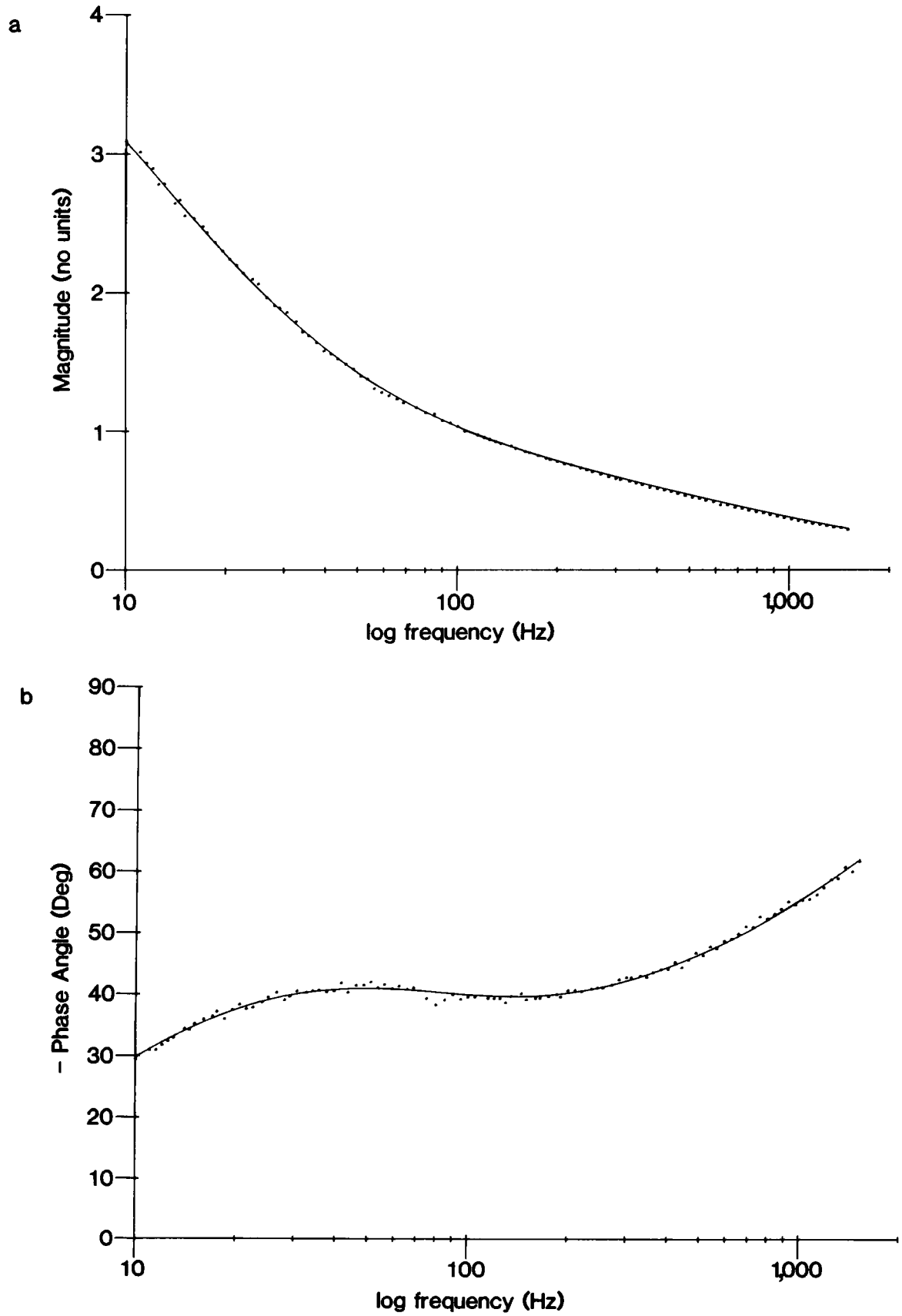

FIGURE 4 Measurement of $V'_1/\Delta V'$ from the center of the fiber. The *upper* panel shows the magnitude of the impedance, the *lower* panel the phase angle. The theoretical curve and fitting procedure is described in the text.

TABLE I
CURVE FIT RESULTS AT CENTER OF THE FIBER

Fiber	Resting potential	Surface membrane specific resistance, R_m	Resistivity of lumen of T system, R_L	Surface membrane specific capacitance, C_m	T system membrane specific capacitance, C_T	Interfiber resistance, R_f	Interfiber spacing, δ
	mV	*Ω-cm²*	*Ω-cm*	*μF/cm²*	*μF/cm²*	*Ω-cm*	*μm*
1	−78	2,200	170	2.6	0.72	9,000	0.10
2	−79	4,100	230	2.4	0.62	11,900	0.10
3	−83	5,400	200	2.0	0.77	5,000	0.27
4	−80	5,700	120	1.1	0.84	1,900	0.83
5	−81	3,600	100	1.3	0.91	2,700	0.57
6	−85	2,500	210	2.3	0.81	10,100	0.11
7	−84	4,400	80	3.3	0.73	5,700	0.28
8	−81	3,000	90	3.1	0.74	9,800	0.14
mean	−81	3,900	150	2.3	0.77	7,000	0.30
SEM	1	464	21	0.3	0.03	1,430	0.27

Temperature = 22°C, sarcomere length = 2.8 μm. Fits include a resistance of 100 Ω (for 1 cm fiber length) in series with bare membrane (Fig. 12). Interfiber spacing (δ), calculated from Eq. A5; resistivity of bathing solution assumed to be 80 Ω cm; T system membrane specific resistance assumed to be 50 kΩ cm (Eisenberg and Gage, 1969).

z_i, as a function of frequency (see Eqs. 9 and 10). Fig. 5 shows such a plot for a representative fiber. Note the phase angle is nearly zero except at highest frequencies, where we feel the nonzero estimates are most likely the result of experimental errors. The phase angle is computed as the difference between two large numbers, so small fractional errors in measurement become a large fractional error in the result. The measurements are also subject to a systematic error of a few degrees (in the negative direction) produced by the lumped resistance of the bath and/or bath electrode.

The estimate of r_i, namely the real part of z_i, and the measured fiber diameter were used to estimate the resistivity of the sarcoplasm R_i of each fiber. The average value of R_i for the eight fibers (165 ± 23 Ω cm, close to the more carefully measured value of Hodgkin and Nakajima (1972) namely, 169 Ω cm) was then used with the measured value of the resistance per unit length r_i to estimate the apparent circular radius for the fiber (mean = 63 ± 4 μm).

A structural model of the electrical properties of the fiber was constructed using the mesh model of the T system of Mathias et al. (1977) but including potential drops in the space between neighboring fibers (see Appendix). This model was fit to the measured data $V_1'/\Delta V'$ in the frequency range 10–1,500 Hz, using the measured electrode spacings and the morphometric parameters of Mobley and Eisenberg (1975). Data below 10 Hz were not used because of the recent description (Valdiosera et al., 1983) of reactance in this frequency range not described by our model.

Our estimates of the specific resistance of the surface membrane, R_m, agree well with those of other investigators; however, our values of surface capacitance, C_m, were higher and our value of tubular membrane capacitance, C_T, were lower than have generally been found (Schneider, 1970; Valdiosera et al., 1974*c*; Mathias et al., 1977), probably because of the different treatment of the resistance of the clefts between the fibers. The values of interfiber resistance, R_f, and the calculated average interfiber spacing of 0.3 μm are in agreement with the morphology. The estimate of the resistivity of the solution in the lumen of the tubules R_L = 160 Ω cm agrees well with earlier work (e.g., Mathias et al., 1977) but is significantly higher than the resistivity of the bathing solution (~80 Ω cm). The high value could be explained if most radial current flowed through paths containing tubules of nonuniform diameter (Eisenberg, 1984*a*). If that were the case, morphological measurement would be dominated by the more common and more easily observed large size T tubules, for example, those which form the central element of the triad. On the other hand, the radial resistance to current flow would be dominated by narrow T tubules (for example, those running from the triad of one myofibril to the triad of the radially adjacent myofibril) because current flow is controlled by a high value resistor in series with a low value resistor. Thus, the radial resistance of a T system consisting of nonuniform tubules would be larger than the resistance computed from a network of uniform tubules with the average morphometric parameters of the nonuniform network.

Electrodes at the End of the Fiber: Traditional Analysis

Complexities became apparent when a procedure analagous to that just described was applied with the microelectrodes impaled near the fiber end (see Fig. 1) and the longitudinal current at the end of the fiber was assumed to be zero. Eqs. 15 and 14 (with y_{en} = 0) were used to

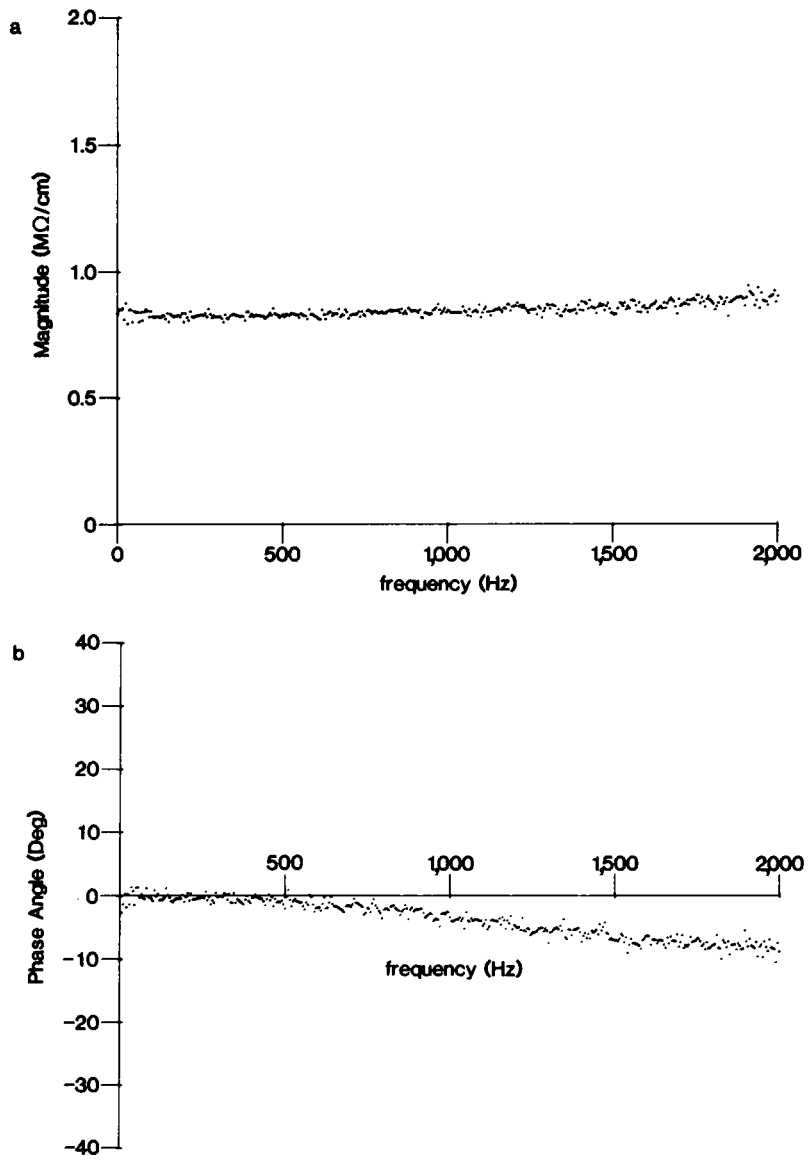

FIGURE 5 Sarcoplasmic impedance z_i estimated near the center of the fiber. The *top* panel is the magnitude and the *bottom* panel is the phase angle. The deviation in phase angle from 0° at high frequencies is likely to be the result of experimental error.

generate plots of the fiber's sarcoplasmic impedance, z_i, as a function of frequency from measurements of $V_1/\Delta V$ and V_1/I_0. The phase angle estimated this way is between 5 and 10° in the low frequency region where the measurements are thought to be reliable (Fig. 6). On the other hand, the equivalent measurements in the middle of the fiber give a zero phase angle (Fig. 6). Previous experiments have also shown that the sarcoplasmic impedance in the middle of the fiber has zero phase angle (Mobley et al., 1974, 1975) and so we must question the assumptions that led to the results of a nonzero phase angle in z_i at the end of the fiber.

Other analysis using the traditional assumption of negligible current flow at the end of the fiber also led to difficulties. Measurements of $V_1/\Delta V$ were used to determine the parameters of a structural model of the muscle fiber much as they had been in the center of the fiber.[1] The fit of theory and data was satisfactory but the estimates of the parameters of the fiber were different from those made in the middle of the fiber (Table II): the estimate of the resistivity R_L of the T lumen was much too low and the estimate of the specific capacitance of the T membrane was too high.

The extra capacitance estimated from measurements at the end of the fiber suggests a possible explanation of all the difficulties. Extensive folding of the outer membrane at the myotendon junction (Eisenberg and Milton, 1984) might provide a pathway for significant longitudinal cur-

[1]At the fiber end, diameters were measured optically and the sarcoplasmic resistivity, R_i, was set equal to the value measured in the middle of fibers.

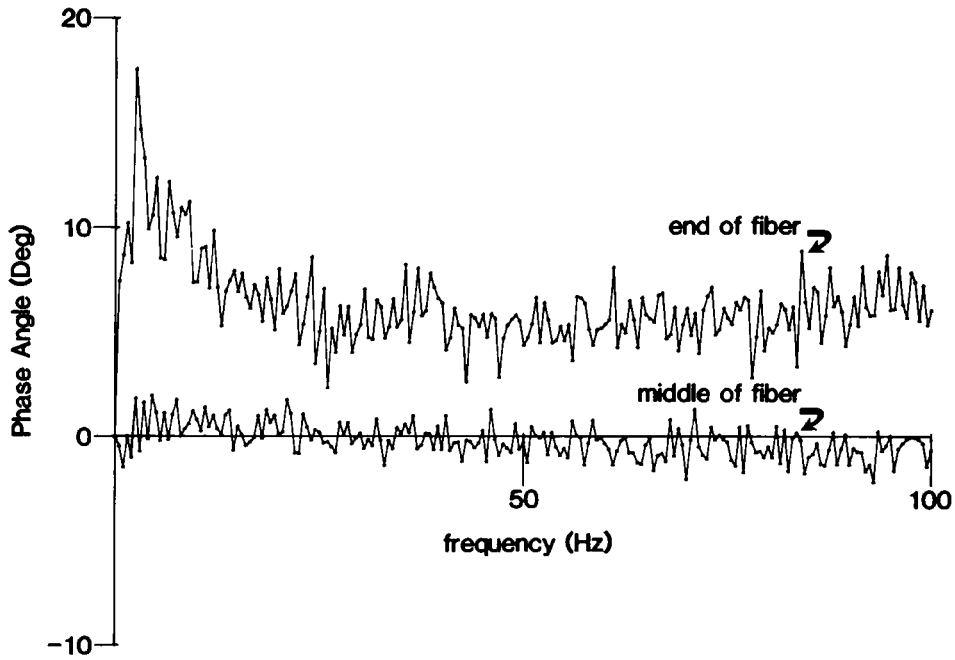

FIGURE 6 Measurement of phase angle of fiber sarcoplasmic impedance at fiber center (fiber No. 3) and fiber end (fiber No. 1). The phase angle of z_i is subject to experimental uncertainties above 100 Hz (see Discussion) and so is not presented.

rent flow out the end of the fiber, thus falsifying the traditional assumption of negligible longitudinal current at the end. The extra membrane involved in these folds would introduce a substantial capacitance that is misrepresented in traditional analysis as extra tubular capacitance and reduced luminal resistance. Computer simulations show that capacitive current flow at the end of the fiber also introduces a phase shift in the longitudinal current flow in the fiber, which in turn appears as an apparent phase shift in the longitudinal impedance in models that assume no current flow at the fiber end.

The rest of our experiments were designed to measure the electrical properties of the myotendon junction using models that explicitly allow current flow out the end of the fiber. Results determined from the later analysis supplant the estimates shown in Table II which were made with an incorrect model.

Measurements at the End of the Fiber: Complete Analyis

The theory of current flow at the end of the fiber was modified to include the admittance y_{en} (see Theory); the

TABLE II
CURVE FIT AT END OF FIBER*

Fiber	Resting potential	Surface membrane specific resistance, R_m	Resistivity of lumen of T system, R_L	Surface membrane specific capacitance, C_m	T system membrane specific capacitance, C_T	Interfiber resistance, R_f	Interfiber spacing, δ
	mV	Ω-*cm*²	Ω-*cm*	μ*F*/*cm*²	μ*F*/*cm*²	Ω-*cm*	μ*m*
1	−81	7,400	78	1.9	1.3	1,800	0.72
2	−81	4,700	52	0.6	1.4	1,100	1.14
3	−80	4,800	33	1.6	1.5	900	1.75
4	−83	4,800	89	3.2	0.9	3,900	0.28
5	−88	3,800	55	3.4	1.0	2,300	0.47
6	−84	2,100	44	3.2	1.2	4,500	0.22
7	−83	4,800	36	0.4	1.6	550	2.55
8	−78	1,600	30	3.3	1.0	4,400	0.27
mean	−82	4,200	60	2.5	1.2	2,300	0.93
SEM	1	636	11	0.4	0.1	530	0.30

See notes to Table I. These estimates are supplanted by Tables III and IV.
*Assuming end of fiber admittance equals 0.

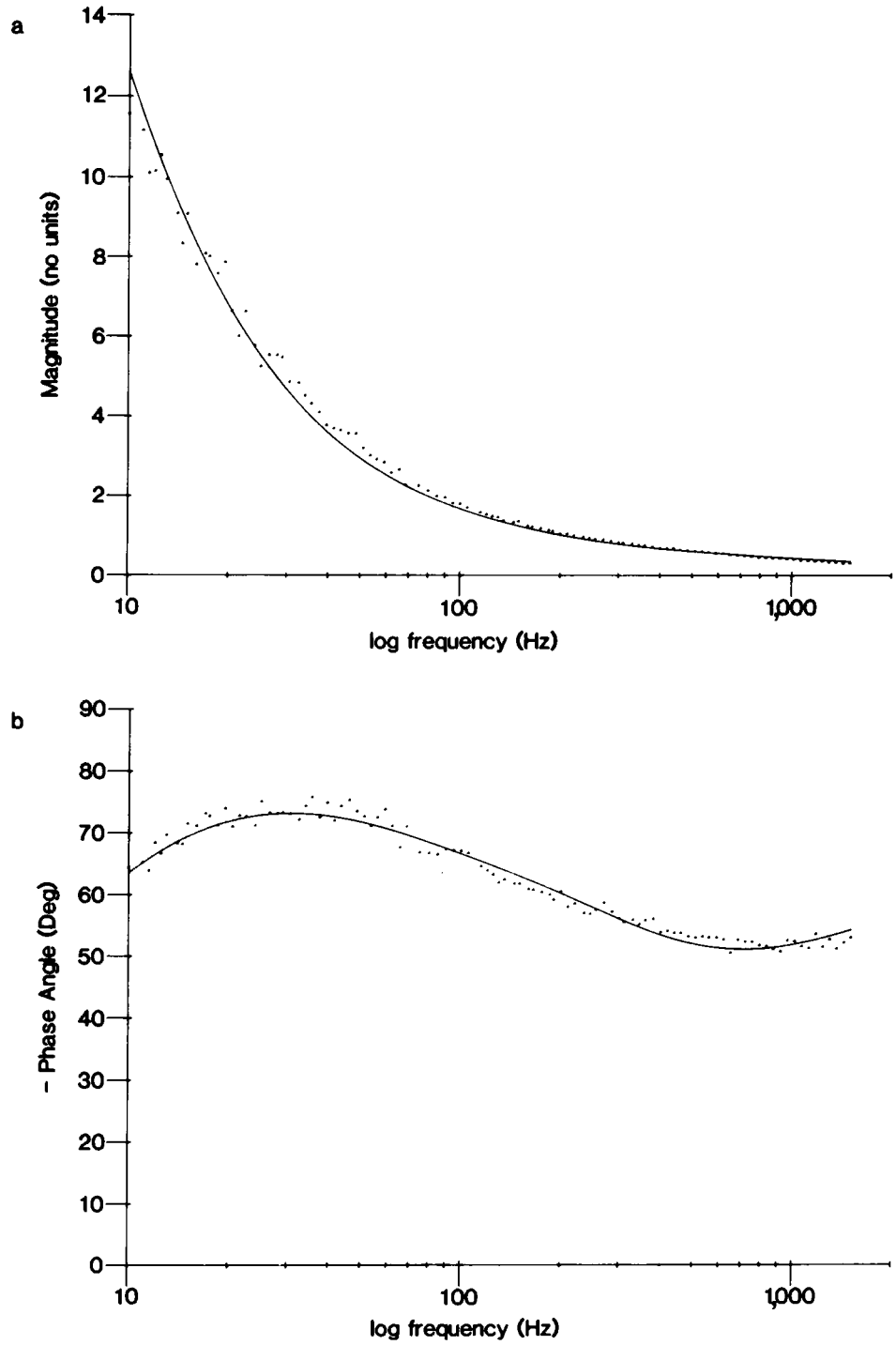

FIGURE 7 Measurement of $V_1/\Delta V$ from the end of the fiber. A theoretical model including a a nonzero end of fiber admittance was fit to this data, as described in text. The *upper* panel shows the magnitude of the impedance and the *lower* panel shows the phase angle.

end of the fiber was represented by a parallel combination of a resistor and capacitor in series with an access resistance (Fig. 3); and methods were developed to estimate the electrical parameters of the fiber, the fiber end, the outer membrane, and the tubular system.

Fits of the complete theory to impedance measurements did not satisfactorily determine all the parameters because three new parameters are more than can be determined independently with the curve-fitting procedure. We therefore determined the values of C_m, R_L, and C_T by impaling fibers near their center and then other fibers, of the same muscle, at their end. Unfortunately, the overlapping of fibers made it impossible to record from the same fiber in center and end. The complete theoretical model including y_{en} was now fit (Fig. 7: parameter values in Table III) to measurements of $V_1/\Delta V$, using values of C_m, R_L, and C_T

TABLE III
END OF FIBER CURVE FIT RESULTS

Fiber	Optically measured radius, a	Surface membrane resistance, R_m	Capacitance of fiber end for a unit cross-sectional area C_{en}	Conductance of fiber end for a unit cross-sectional area G_{en}	Series resistance of fiber end for a unit cross-sectional area, R_{se}	Interfiber resistance, R_f	Interfiber spacing, δ
	μm	Ω-cm^2	$\mu F/cm^2$	mS/cm^2	Ω-cm^2	Ω-cm	μm
1	62	5,900	40	0.16	3.9	500	2.51
2	60	6,300	42	0.68	3.3	1,700	0.74
3	75	7,100	56	0.41	1.5	500	3.14
4	53	5,900	41	0.81	1.7	5,900	0.19
5	42	4,100	49	0.24	0.9	2,100	0.42
6	48	2,500	65	1.56	0.3	2,500	0.40
7	67	6,700	60	0.52	3.8	1,300	1.08
8	56	1,900	47	1.07	0.8	800	1.47
mean	58	5,000	50	0.68	2.0	1,900	1.24
SEM	4	707	3	0.2	0.5	601	0.38

Fixed parameter values: $C_m = 2.3\ \mu F/cm^2$; $C_T = 0.77\ \mu F/cm^2$; $R_L = 150\ \Omega$ cm; See notes of Table I.
*Assuming end of fiber admittance does not equal 0.

previously determined from measurements near the center of the fiber.

The most notable result of these curve fits is the high value of capacitance C_{en} at the fiber end. If the membranes at the fiber end have a specific capacitance of 1 $\mu F/cm^2$, our result implies a membrane area at the end of the fiber some fifty times larger than the cross-sectional area of the fiber.

The value of the conductance of the membranes at the myotendon junction G_{en} is not so reliably determined by the curve fits. If G_{en} is constrained to a very small value (<1 $\mu S/cm^2$), the curve-fitting procedure produces an estimate of R_m smaller by ~20%, while the quality of the fit and the estimate of the other parameters were essentially unaffected. If G_{en} is constrained to a value of some 2.5 mS/cm^2, the estimates of R_m became unreasonably high (>20 $k\Omega$-cm^2) and the fits became noticeably worse. For that reason we think our results bound G_{en} between zero and some 2.5 mS/cm^2. If our estimate of the amount of membrane at the fiber end is correct, the estimate of G_{en} implies that the membranes at the tendon junction have a specific resistivity >20 $k\Omega$-cm^2, suggesting that these membranes contain few open ionic channels under our experimental conditions. The value of the outer membrane resistance, R_m, at the fiber end was somewhat higher than that obtained in the fiber middle, suggesting that there are also fewer open ionic channels in the surface membrane near the tendon junction.

The effective interfiber resistance, R_f, was much lower at the end of the fiber than in the center, suggesting that muscle fibers become less densely packed as they approach the myotendon junction. We do not know if this is a peculiarity of the sartorius muscle of *Rana temporaria* or a necessary consequence of the structure of the muscle/tendon insertion.

The resistance in series with a unit of cross-sectional area at the myotendon junction, R_{se}, is unexpectedly high. A convergence resistance to the fiber end would account

TABLE IV
DIRECT MEASUREMENT OF END OF FIBER ADMITTANCE, y_{en}

Fiber	Resting Potential	Measured diameter	r_i	R_i	Calculated radius	C_{en}	G_{en}	R_{se}
	mV	μm	$M\Omega/cm$	Ω-cm	μm	$\mu F/cm^2$	mS/cm^2	Ω-cm^2
1	−83	65	3.5	115	38	28	−3.5	2.6
2	−85	105	1.4	117	61	69	1.7	3.5
3	−84	134	1.5	214	57	19	−1.0	4.1
4	−79	143	1.5	239	59	42	−2.7	4.4
5	−79	126	1.8	229	52	83	1.1	3.6
6	−81	116	0.82	86	78	102	6.2	2.3
7	−84	109	1.1	98	69	42	1.4	3.9
mean	−82			157		55	0.5	3.5
SEM	1			25		11	1.3	0.3

r_i = average value between 50–100 Hz; C_{en}, G_{en}, R_{se}, see Eq. 4.

for ~0.2 to 0.3 Ω cm^2 of series resistance, an order of magnitude less than our result, suggesting that myotendon membrane current flows to the bathing solution through a narrow elongated pathway.

The need to set three of the electrical parameters in order to fit our theory was somewhat unsatisfactory, even though the values chosen were experimentally measured. We therefore made direct measurements (Table IV; Fig. 8) of the admittance at the end of the fiber by the method outlined in the Theory section: Γ was determined from Eq. 9, then substituted into Eq. 16 and 17, which in turn were combined to give an estimate of y_{en} at each frequency; C_{en} and R_{se} were then determined from Eq. 4. These values agree well with those obtained by the curve fits and were quite robust: they are insensitive to known errors.

Estimates of G_{en}, on the other hand, are sensitive to errors in locating the end of the fiber. Fairly small changes in the estimate of $-L$ could change the sign of the conductance! Furthermore, the estimates of G_{en} depend mostly on data taken at very low frequencies (because only then does the resistive current dominate the capacitive current through the myotendon membrane). The signal-to-noise ratio of the signal $V_1/\Delta V$ at these frequencies is poor, however, because the length constant at low frequencies is large and the longitudinal potential drop ΔV is tiny. This latter error was minimized by estimating $(\pi a^2)G_{en}$ from the average of the real part of y_{en} between 5 and 25 Hz (Eq. 4). Both types of error could cause the negative values of G_{en} reported in Table IV; nonetheless, the direct estimates of G_{en} support the conclusion that the myotendon membrane contains few open channels.

SIMULATIONS

The effects of the capacitance at the end of the fiber were examined in simulations computed with the parameters determined by our impedance measurements. The first point examined was the effect of current flow at the end of the fiber on the uniformity of potential near the fiber end. Fig. 9 shows the longitudinal distribution of potential in the presence and absence of current out the end of the fiber; note the negligible effect at zero frequency (when little current flows through the very high resistance membranes at the myotendon junction) and the large effect at 100 Hz, when substantial current flows through the capacitance of the membranes at the myotendon junction.

Fig. 10 shows simulations of current flow in a muscle fiber made with a lumped model of the T system (Mathias et al., 1977) and with electrode locations L_2 = 400 μm; and L_1 = 200 μm. The membrane current estimated by the voltage difference ΔV (the traditional estimator of membrane current) is not a good approximation to that which actually flows. The integral of the transient current, which is the traditional estimator of the total fiber capacitance and total membrane area, would be 1.7 times the actual capacitance in this case.

Fig. 11 shows that measurements of nonlinear charge movement are not seriously corrupted by the large errors seen in Figs. 9 and 10, if the capacitance at the myotendon junction is assumed to be strictly independent of voltage. The simulation shown represents nonlinear charge movement by placing a series RC element in parallel with the T membrane circuit element when the T membranes were

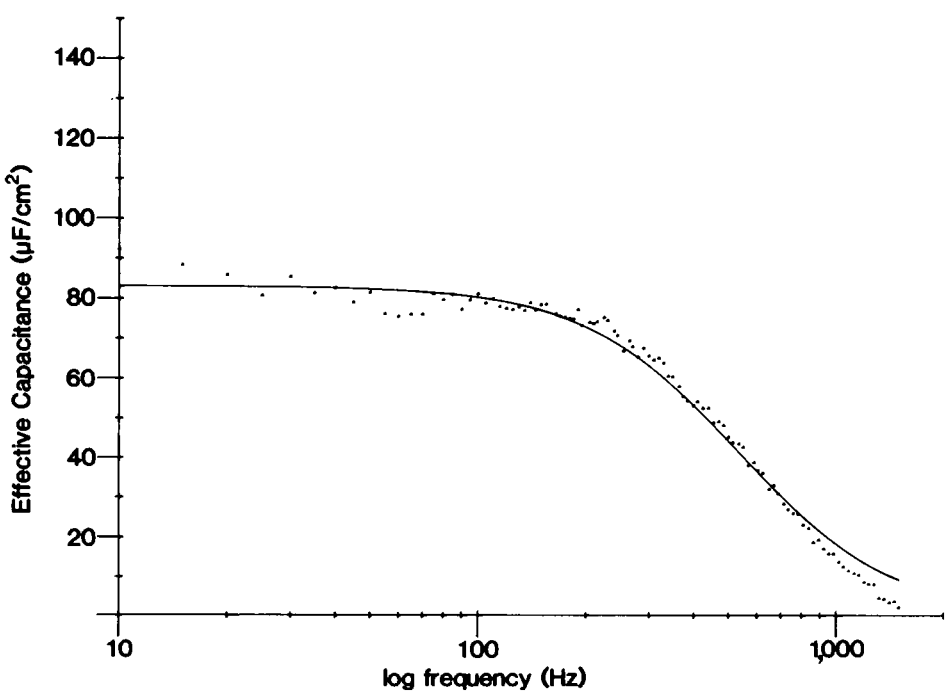

FIGURE 8 Direct measurements of the admittance of the end of the fiber, $Im(y_{en}/\omega)$. Theoretical curve calculated from the circuit model shown in Fig. 3 (see text).

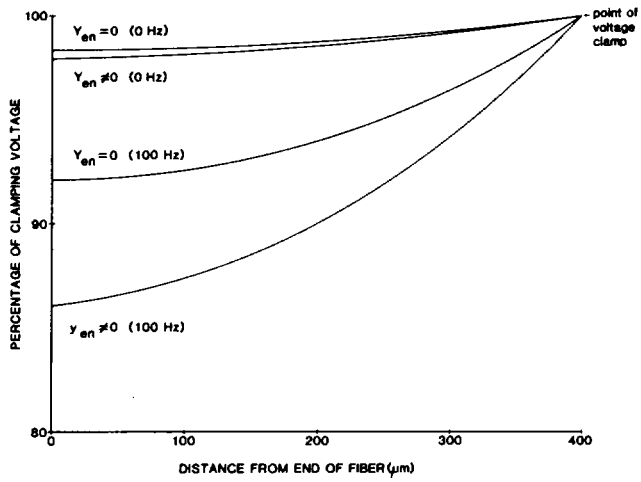

FIGURE 9 Predicted decrement in voltage with distance. Calculated using Eq. 12, with average parameter values from Tables III and IV.

depolarized (compare the Appendix of Mathias et al., 1980). The current record shown is just the nonlinear component of the response. It is computed by adding the inward current flowing in response to a hyperpolarizing step applied to the circuit without the series $R_Q C_Q$ element to the outward current flowing in response to a depolarizing step applied to the circuit with the series $R_Q C_Q$ element. The near identity of the records shows that current flow at the end of the fiber has little qualitative effect on the nonlinear current estimated by the end of the fiber voltage clamp method.

The estimates of nonlinear capacitive current are not very sensitive to current flow out the end of the fiber for several reasons. First, spatial control of intracellular and tubular potential is most easily obtained for small passive currents like nonlinear charge movement (Levis et al., 1983). Second, the time course of charge movement is slow compared with the time necessary to achieve longitudinal control of intracellular potential (Kootsey and Johnson, 1972; Kootsey, 1975) or radial control of tubular potential (Levis et al., 1983). Third, the component of current flow that is in error, namely, the linear component of current measured with the hyperpolarizing voltage step, is subtracted from the final result.

DISCUSSION

Experimental Uncertainties

The location of the end of the fiber is subject to experimental uncertainty owing to the limitations in visibility and the taper of the fiber near the myotendon junction. The location is subject to conceptual difficulty because morphological techniques do not tell us where the density of channels changes from its value in the center of the fiber (giving specific resistance, R_m) to that at the end of the fiber (giving the conductance G_{en}). The operational definition of the end of the fiber should be chosen to minimize the errors in estimates of electrical parameters. If the taper extended uniformly over just one fiber diameter, the operational definition used here (namely, one radius from

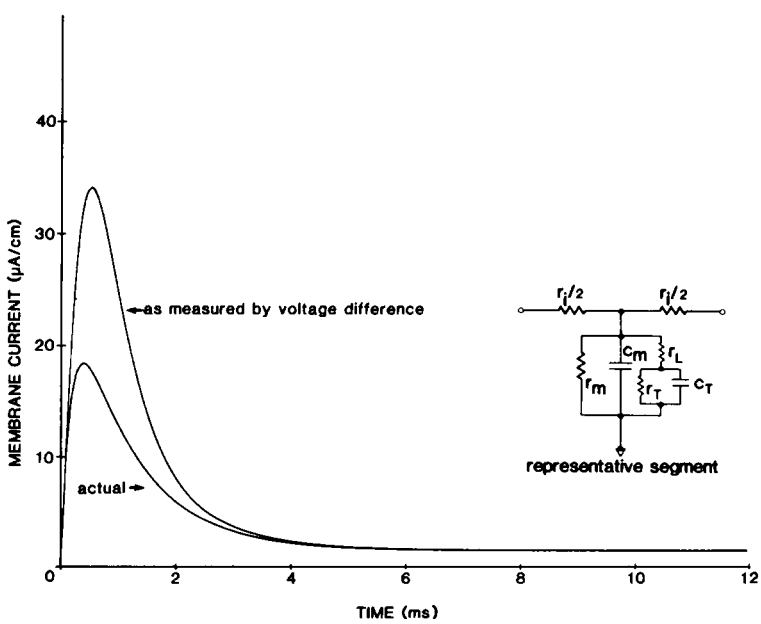

FIGURE 10 Simulations showing difference between actual membrane current and current estimated by classical methods. The actual current was that flowing across the membrane at $x = -L_1$. The classical current was measured by the voltage difference $2\Delta V/[r_i(L_1^2 - L_2^2)]$. The fiber was divided into segments 40 μm in length and the T system was represented as a lumped model. Parameters were electrode separations $L - L_2$ and $L_2 - L_1 = 200$ μm; resistance and capacitance of a unit length of outer membrane 100 kΩ cm and 87 nF/cm; $r_i = 5.7$ kΩ cm, resistance of the lumen of tubules in a unit length of fiber 200 kΩ cm; capacitance of tubular membranes in a unit length of fiber 0.19 μF/cm. The actual effective capacitance was 0.268 μF/cm and the effective capacitance measured by classical methods was nearly twice that, namely, 0.456 μF/cm (see Milton, 1984, for definitions and detailed discussion of effective capacitance).

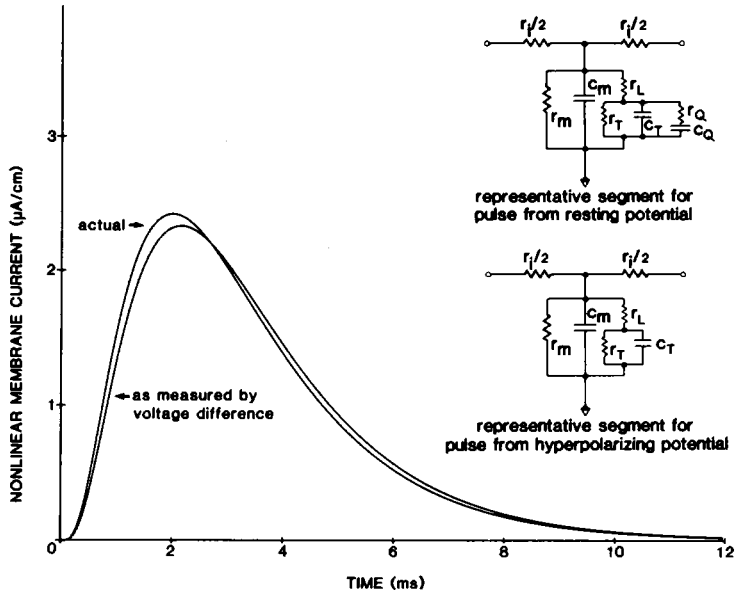

FIGURE 11 Simulations showing actual nonlinear charge movement and nonlinear charge estimated by classical methods. The fiber was divided into segments 40 μm in length. Charge movement was calculated from a lumped model of the T system (see text) to which a series RC element was added when a depolarization test pulse of 100 mV was applied. The currents shown are computed by the classical procedure: they represent the difference between the response of the circuit to a depolarization and the voltage-independent response to an identical voltage step. The parameters used were $r_m = 1 \times 10^5\ \Omega$ cm, $c_m = 8.7 \times 10^{-8}$ F/cm, $r_L = 5.7 \times 10^3\ \Omega$ cm, $r_T = 2 \times 10^5\ \Omega$ cm, $c_T = 1.9 \times 10^{-7}$ F/cm, $r_Q = 1 \times 10^6\ \Omega$ cm, $c_Q = 1 \times 10^{-8}$ F/cm.

the fiber end) would be appropriate. More precise measurements of the taper, made after the experiments reported here (Eisenberg and Milton, 1984), show that the taper extends roughly two diameters, so a better definition would be one diameter from the absolute end. If, on the other hand, the electrical end were operationally defined as the furthest point of the fiber seen in the microscope (as may well have been done in published experiments that do not comment on this problem), substantial errors would result: the capacitance of the surface and tubular membranes would be underestimated by 40% for an electrode spacing of 200 μm. This underestimate would mask the capacitance of the folded membranes at the myotendon junction. In any case, these uncertainties are intrinsic to quantitative estimates made with the end of the fiber voltage clamp.

Effects of Interfiber Resistance

The Appendix demonstrates that the resistance between muscle fibers can be substantial; and curve fits of models with and without this resistance suggest a substantial effect on estimates of membrane capacitance. When the interfiber resistance is not included, the surface membrane appears to have some 0.8 μF/cm^2 capacitance, in agreement with earlier workers (e.g., Schneider, 1970; Valdiosera et al., 1974*c*; Mathias et al., 1977). When reasonable estimates of the interfiber resistance are included, the surface membrane appears to have a capacitance of some 2.3 μF/cm^2. This latter figure is easily explained if the caveolae of the outer membrane (Dulhunty and Franzini-Armstrong, 1975) are in series with a negligible resistance and thus contribute directly to the surface capacitance. It seems clear, however, that experiments designed to provide quantitative estimates of membrane properties are best done on isolated fibers in which the extracellular potential can be minimized.

Effects on Classical Measurements

The measurements and simulations in this paper evaluate the assumptions underlying the end of the fiber voltage clamp technique. Our results demonstrate that the main assumption—of negligible longitudinal current flow at the end of the fiber—is inaccurate; and the simulations demonstrate the consequences of this inaccuracy.

The main effect of longitudinal current flow at the end of the fiber is on estimates of the linear (i.e., voltage independent) properties of the fiber. These estimates are in serious error if current flow out the end of the fiber is neglected.

The effects on estimates of nonlinear properties are more subtle. In the idealized case, where the capacitance at the end of the fiber is strictly voltage independent, classical estimates of nonlinear properties are not in error in themselves because the linear properties (subject to large error) are subtracted. However, most estimates of charge movement properties in the literature are divided by estimates of the total capacitance of the fiber in an attempt to normalize results to the area of T membrane. As it turns out, normalization of this type contaminates otherwise accurate

measurements of nonlinear properties with the substantial inaccuracy of the linear measurements.

Voltage clamp studies in which the electrodes are moved (see Adrian and Almers, 1976) are particularly subject to error. Although we have not simulated such studies directly, our analysis and simulations show that estimates of membrane current flow are critically dependent on electrode separation when current flows out the end of the fiber. Thus, measurements involving more than one set of electrode locations are likely to be misleading if they are interpreted with the classical assumption of no current flow out the end of the fiber.

Our results and simulations have not addressed the question of the adequacy of control of potential in the presence of large inward membrane currents (Kootsey and Johnson, 1972: Kootsey, 1975; Levis et al., 1983). It is clear, however, that the large value of C_{en} reported here precludes rapid control of the intracellular potential. Thus, fast currents, even if they are generated entirely by channels in the surface membrane, cannot be studied at the end of the fiber.

CONCLUSION

The main conclusion of these experiments is that the end of the muscle fiber has a large extra capacitance produced, in all likelihood, by the folded membrane at the myotendon junction. This extra capacitance introduces substantial ambiguities into the interpretation of voltage clamp measurements made at the end of the fiber even if the extra capacitance is assumed to be strictly independent of voltage. Other uncertainties arise from the ambiguities in locating the anatomical end of the fiber. Finally, we must remember the devastating possibility of charge movement (i.e., voltage-dependent capacitance) in the membranes at the myotendon junction. Combined, these uncertainties suggest that quantitative voltage clamp measurements be made away from the myotendon junction, if possible.

APPENDIX

Interfiber Resistance

The outer membranes of a muscle fiber on the surface of a bundle or whole muscle can be divided into two sections; those that face the bathing solution and those that face the narrow clefts between adjacent fibers. The overall pattern of current from these two sections will depend on the resistance of the narrow clefts, the interfiber resistance.

An approximate analysis is presented here to show the qualitative effects expected. We represent a surface fiber as shown in Fig. 12, with half the fiber directly facing the bath and the other half facing its neighbors. Kirchoff's current law and Ohm's law can be applied to the infinitesimal segment of interfiber space with $\Delta\phi \rightarrow 0$ to give the transmission line equation for the extracellular space

$$u(\phi, s) = \frac{\delta}{\rho Y_m(s)} \frac{d^2 u(\phi, s)}{d\phi^2} \tag{A1}$$

and the boundary conditions for the symmetrical problem are

$$u(\phi, s) = V_m(s) \text{ at } \phi = \pi a/2$$

$$\text{and} \quad \frac{du(\phi, s)}{d\phi} = 0 \text{ at } \phi = 0, \tag{A2}$$

where j_m is the Laplace transform of membrane current density at the angular location (ϕ amperes per centimeter squared), $u(\phi, s)$ is the Laplace transform of the potential across the fiber membrane, namely, $u(\phi, s) = V_m(s) - V_\delta(\phi, s)$, $V_\delta(\phi, s)$ is the Laplace transform of the voltage in the interfiber space, the bath being called zero (in volts), $V_m(s)$ is the Laplace transform of the voltage within the fiber (in volts), Y_m is the specific membrane admittance of fiber (in siemens per centimeter squared), s is the Laplace transform variable, a generalization of frequency (in hertzs or seconds^{-1}), δ is the spacing between fibers (in centimeters), $\gamma(s) = \sqrt{\rho Y_m/\delta}$, and ρ is the resistivity of solution in the interfiber space in ohms per centimeter. The solution satisfying Eqs. A1 and A2 is

$$u(\phi, s) = \frac{V_m(s)}{\cosh\left[\frac{\gamma(s)\pi a}{2}\right]} \cosh[\gamma(s)\phi]. \tag{A3}$$

The total current, I_m, leaving a unit length of fiber is the sum of the current leaving the bare side of the fiber, namely, $\pi a Y_m V_m$, and the

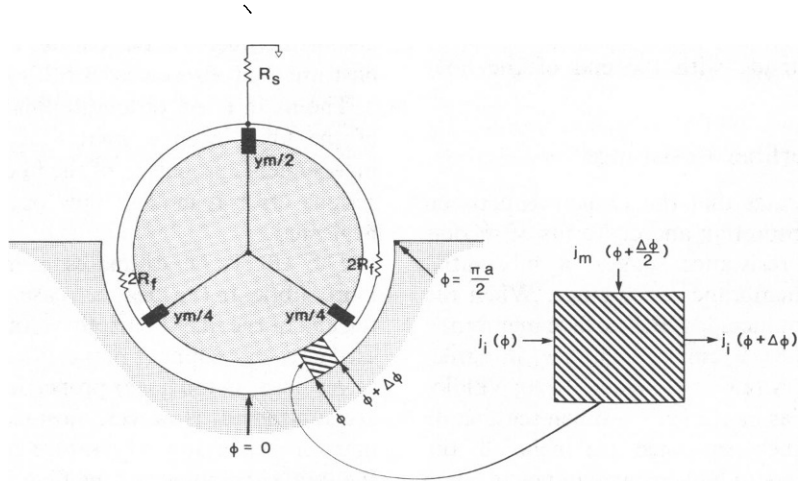

FIGURE 12 Circuit model representing muscle fibers packed into a muscle.

current leaving the clefts, namely, twice the integral (from $\phi = 0$ to $\phi = \pi a/2$) of the cleft membrane current

$$I_m = 2\int_0^{\pi a/2} j_m(\phi, s)\,d\phi + \pi a Y_m V_m$$
$$= Y_m V_m\left[\pi a + \frac{2}{\gamma(s)\coth(\pi\gamma a/2)}\right]. \quad \text{(A4)}$$

Using the approximation $\coth\theta \approx (1/\theta) + (\theta/3)$, we have

$$\frac{I_m}{V_m} \approx \pi a Y_m + \frac{\pi a Y_m}{1 + \pi a Y_m\left(\frac{\rho\pi a}{12\delta}\right)},$$

which can be represented by the lumped circuit model shown in Fig. 12.

It is a pleasure to thank Mr. Richard McCarthy and Dr. Brenda Eisenberg for much help and many useful discussions.

The work was supported by grants from the Muscular Dystrophy Association, the American Heart Association, and the National Institutes of Health.

Received for publication 4 January 1985 and in final form 18 March 1985.

REFERENCES

Adrian, R. H. 1984. Electrical properties of striated muscle. *Handb. Physiol. Sect. 10: Skeletal Muscle.* 275–300.

Adrian, R. H., and W. Almers. 1976. The voltage dependence of membrane capacity. *J. Physiol. (Lond.).* 254:317–338.

Adrian, R. H., W. K. Chandler, and A. L. Hodgkin. 1970. Voltage clamp experiments in striated muscle fibers. *J. Physiol. (Lond.).* 208:607–644.

Adrian, R. H., and W. H. Freygang. 1962. The potassium conductance of frog muscle membrane under controlled voltage. *J. Physiol. (Lond.).* 163:104–114.

Almers, W. 1978. Gating currents and charge movements in excitable membranes. *Rev. Physiol. Biochem. Pharmacol.* 82:96–190.

Chandler, W. K., and M. F. Schneider. 1976. Time-course of potential spread along a skeletal muscle fiber under voltage clamp. *J. Gen. Physiol.* 67:165–184.

Dulhunty, A. F., and C. Franzini-Armstrong. 1975. Variations in internal resistivity with sarcomere length in frog semitendinosus fibers. *Biophys. J.* 15(2, Pt. 2):130*a*. (Abstr.)

Eisenberg, R. S., and P. W. Gage. 1969. Ionic conductance of the surface and transverse tubular membranes of frog sartorius fibers. *J. Gen. Physiol.* 53:279–297.

Eisenberg, B. R., and R. L. Milton. 1984. Muscle fiber termination at the tendon in the frog's sartorius: a stereological study. *Am. J. Anat.* 171:273–284.

Eisenberg, R. S. 1984*a*. Impedance measurement of the electrical structure of skeletal muscle. *Handb. Physiol. Sect. 10: Skeletal Muscle.* 301–323.

Eisenberg, R. S. 1984*b*. Membranes and channels. Physiology and molecular biology. *In* Membranes, Channels, and Noise. R. S. Eisenberg, M. Frank, and C. F. Stevens, editors. Plenum Publishing Corp., New York. 235–283.

Hodgkin, A. L., and S. Nakajima. 1972. The effect of diameter on the electrical constants of frog skeletal muscle fibers. *J. Physiol. (Lond.).* 221:105–120.

Horowicz, P., and M. F. Schneider. 1981. Membrane charge movement in contracting and noncontracting skeletal muscle fibers. *J. Physiol. (Lond.).* 314:565–593.

Jack, J. J. B., D. Noble, and R. W. Tsien. 1975. Electric Current Flow in Excitable Cells. Clarendon Press, Oxford.

Kootsey, J. M., and E. A. Johnson. 1972. Voltage clamp of cardiac muscle. A theoretical analysis of early currents in the single sucrose gap. *Biophys. J.* 11:1496–1508.

Kootsey, J. M. 1975. Voltage clamp simulation. *Fed. Proc.* 34:1343–1349.

Levis, R. A., R. T. Mathias, and R. S. Eisenberg. 1983. Electrical properties of sheep Purkinje strands. *Biophys. J.* 44:225–248.

Mathias, R. T. 1984. Analysis of membrane properties using extrinsic noise. *In* Membranes, Channels, and Noise. R. S. Eisenberg, M. Frank, and C. F. Stevens, editors. Plenum Publishing Corp., New York. 49–116.

Mathias, R. T., R. S. Eisenberg, and P. Valdiosera. 1977. Electrical properties of frog skeletal muscle fibers interpreted with a mesh model of the tubular system. *Biophys. J.* 17:57–93.

Mathias, R. T., R. A. Levis, and R. S. Eisenberg. 1980. Electrical models of excitation contraction coupling and charge movement in skeletal muscle. *J. Gen. Physiol.* 76:1–31.

Milton, R. L. 1983. Electrical properties and morphology of the membranes at the myotendon junction. Ph.D. thesis, Rush University, Chicago, Illinois. 108 pp.

Mobley, B. A., J. A. Leung, and R. S. Eisenberg. 1974. Longitudinal impedance of skinned frog muscle fibers. *J. Gen. Physiol.* 63:625–637.

Mobley, B. A., J. A. Leung, and R. S. Eisenberg. 1975. Longitudinal impedance of single frog muscle fibers. *J. Gen. Physiol.* 65:97–113.

Schneider, M. F. 1970. Linear electrical properties of the transverse tubules and surface membrane of skeletal muscle fibers. *J. Gen. Physiol.* 56:640–671.

Schneider, M. F. 1981. Membrane charge movement and depolarization-contraction coupling. *Annu. Rev. Physiol.* 43:507–517.

Schneider, M. F., and W. K. Chandler. 1973. Voltage-dependent charge movement in skeletal muscle: a possible step in excitation-contraction coupling. *Nature (Lond.).* 242:244–246.

Schneider, M. F., and W. K. Chandler. 1976. Effects of membrane potential on the capacitance of skeletal muscle fibers. *J. Gen. Physiol.* 67:125–163.

Valdiosera, R., C. Clausen, and R. S. Eisenberg. 1974*a*. Measurement of the impedance of frog skeletal muscle fibers. *Biophys. J.* 14:295–314.

Valdiosera, R., C. Clausen, and R. S. Eisenberg. 1974*b*. Circuit models of the passive electrical properties of frog skeletal muscle fibers. *J. Gen. Physiol.* 63:432–459.

Valdiosera, R., C. Clausen, and R. S. Eisenberg. 1974*c*. Impedance of frog skeletal muscle fibers in various solutions. *J. Gen. Physiol.* 63:460–491.

Valdiosera, R. F., E. Ramirez, and B. Mendiola. 1983. Low frequency impedance of frog muscle fibers. *Biophys. J.* 41(2, Pt. 2):181*a*. (Abstr.)